

1 A hardware-accelerated particle filter for the geolocation of  
2 demersal fishes  
3

4 Chang Liu<sup>1</sup>, Geoffrey W. Cowles<sup>1</sup>, Douglas R. Zemeckis<sup>2</sup>, Gavin Fay<sup>1</sup>, Arnault Le Bris<sup>3</sup>, Steven  
5 X. Cadrin<sup>1</sup>

6 <sup>1</sup>*Department of Fisheries Oceanography, School for Marine Science and Technology, University of Mas-*  
7 *sachusetts Dartmouth. 836 S Rodney French Blvd, New Bedford, MA 02744, USA*

8 <sup>2</sup>*Department of Agriculture and Natural Resources, Rutgers, The State University of New Jersey. 1623*  
9 *Whitesville Road, Toms River, NJ 08755, USA*

10 <sup>3</sup>*Centre for Fisheries Ecosystems Research, Fisheries and Marine Institute of Memorial University of New-*  
11 *foundland, St. John's, Canada*

12 Corresponding author: Chang Liu, cliu3@umassd.edu

13 **Keywords:** geolocation, demersal fish, fish migration, particle filter, archival tagging, data storage tag,  
14 graphics processing unit

15 **Funding:** Funding for the research conducted as part of this manuscript was provided by NOAA Saltonstall-  
16 Kennedy Grant award NA15NMF4270267. Cod tagging research in the Spring Cod Conservation Zone  
17 was conducted in collaboration with the Massachusetts Division of Marine Fisheries and supported by the  
18 United States Fish and Wildlife Service through the Sportfish Restoration Act and the Massachusetts Marine  
19 Fisheries Institute.

## Abstract

Geolocation is increasingly employed to reconstruct the movements of demersal fishes using data retrieved from electronic archival tags. However, geolocation methods commonly suffer from limitations such as low horizontal resolution of locations, flawed land boundary treatment, and extensive computation time. We addressed these issues using a state-space approach based on the particle filter (PF), and developed a geolocation package with graphics processing unit (GPU) acceleration. Our method focused on application to demersal fish and utilizes comparison of the tag-recorded depth and temperature to the same variables from an unstructured grid regional oceanographic model. A rigorous boundary treatment scheme was implemented to handle regions with complex coastline geometry. Validation exercises using stationary mooring tags and double-electronic-tagged (archival and acoustic tags) Atlantic cod in the Gulf of Maine resulted in <10 km median errors of the estimated tracks. Sensitivity analyses suggest that using 200,000 particles was adequate to stabilize the location track estimation. Acceleration of the particle filter using GPUs resulted in faster processing than the single threaded CPU (central processing unit) implementation, enabling rapid geolocations using consumer grade computer hardware. The geolocation output of each tagged fish includes the most probable track and the associated spatial probability distribution. The resulting PF geolocation package enables high resolution and accelerated geolocation analyses to be performed on affordable consumer-grade computer hardware, resolving the time intensiveness problem of the PF that may have prevented its adoptions in marine animal geolocation. Expanded application of geolocation will yield more reliable migration information to support management. Geolocation results from archival tagging will contribute to our understanding of the spatial ecology of marine species.

## 1 Introduction

Electronic tagging has offered improved fishery-independent insights into behavior and population structure of marine species ([Galuardi and Lam, 2014](#); [Hussey et al., 2015](#)). Two commonly employed variants of electronic archival tags are data storage tags (DSTs) and pop-up satellite archival tags (PSATs). These are relatively compact devices that can be attached to a fish and are capable of recording key environmental

45 data such as pressure (i.e., depth), light level, and temperature at precise time intervals, typically seconds to  
46 minutes. These data may be used to estimate locations and possible migration paths of the tagged individual  
47 through geolocation. The majority of geolocation methods for tracking individual aquatic animals use GPS  
48 and light level (Galuardi and Lam, 2014). However, due to attenuation in the water column, these signals  
49 are not suitable for geolocation of demersal species that reside at depth on or near the bottom of the water  
50 column. For demersal fish, geolocation using tag-recorded depth and temperature data is a more appropriate  
51 approach and has been incorporated into several methods, including Metcalfe and Arnold (1997); Hunter  
52 et al. (2003); Andersen et al. (2007); Righton and Mills (2008); Pedersen et al. (2008). Many of these prior  
53 approaches are based on state-space models that account for uncertainties related to the observations and  
54 the estimated quantities (Pedersen et al., 2008; Thygesen et al., 2009; Patterson et al., 2008; Jonsen et al.,  
55 2013).

56 The particle filter (PF), also known as sequential importance resampling or sequential Monte Carlo, is  
57 a statistical method that is commonly applied to tracking applications in fields such as robotics and image  
58 processing (Gustafsson et al., 2002). The PF has also been employed for fish geolocation using archival  
59 tagging data (Nielsen, 2004; Royer et al., 2005; Andersen et al., 2007; Brickman and Thorsteinsson, 2008;  
60 Coleman, 2015), where the possible geographic location of the fish is modeled by an ensemble of samples, or  
61 particles, filtered by the likelihood distributions in an iterative manner. An approach that has been more  
62 widely applied to the archival tagging geolocation problem is the hidden Markov model (HMM). HMMs  
63 typically require a known, finite number of states, thus the HMM-based geolocation methods operate on  
64 a horizontal regular rectangular grid. HMM-based geolocation software packages have been developed and  
65 made available by several research groups (e.g., Pedersen et al. 2008, 2011a; Liu et al. 2017; Braun et al.  
66 2018). In comparing these two methods, the PF has two key advantages over the HMM-based methods for  
67 state-space modeling in the context of the geolocation problem. The first is that the PF is better suited for  
68 filtering both nonlinear and non-Gaussian probability density distributions for the horizontal locations. This  
69 is particularly advantageous for handling simulations when the fish is in coastal waters near land (Andersen  
70 et al., 2007) where Gaussian distributions are not suitable. In the PF, confinement to the domain can be  
71 implemented in a straightforward and robust manner. The second advantage of the PF over HMM-based

72 geolocation is that the PF assumes a continuous state space for particle locations, i.e., modeled particle  
73 locations are not constrained to a finite set of discrete grid points of an underlying horizontal grid. This  
74 avoids the need for any interpolation or discretization of the 2-D spatial distributions onto fixed grids as  
75 required by the HMM approach, which may lead to information loss and render geolocation results dependent  
76 on the horizontal resolution.

77 Previous studies identified that a major drawback of the PF is that it can be computationally intensive  
78 due to the large number of particles needed for a given simulation (Pedersen et al., 2008; Thygesen et al.,  
79 2009; Woillez et al., 2016). This is likely the reason why the PF has been infrequently employed in geolocation  
80 studies despite the clear benefits of the approach. Fortunately, the nature of the PF algorithm enables the  
81 employment of modern computer hardware acceleration approaches to significantly reduce the computation  
82 time. The parallelization of the PF algorithm using multiple CPU cores or graphics processing units (GPU)  
83 to reduce runtime has been studied in the context of other applications (Hendeby et al., 2010; Goodrum  
84 et al., 2011). A GPU is a computer hardware device that was traditionally used to create images to be  
85 rendered on a display. Over the last two decades, software tools and algorithms have been developed to  
86 enable GPUs to be used to accelerate general purpose scientific computation (Vuduc and Choi, 2013). GPUs  
87 typically contain 100s to 1,000s of processing elements (cores) that can perform simple computations in  
88 parallel. Parallelization of the particle filtering problem can be implemented straightforwardly by taking  
89 advantage of the independence of the particles. The lack of interaction between particles allows processing  
90 elements to handle particles or groups of particles without incurring overhead costs related to exchanging  
91 information among particles. In contrast, the HMM geolocation approach is less amenable to straightforward  
92 parallelization and is thus less likely to benefit from modern hardware acceleration approaches.

93 The primary objective of this work was to develop an efficient geolocation method based on the PF for  
94 demersal fishes using archival tagging data. The approach builds from previous work on an HMM-based  
95 model (HMM Geolocation Toolbox, Liu et al. (2017)) and PF models (Royer et al., 2005; Andersen et al.,  
96 2007), and improves on some of the algorithmic deficiencies from these prior efforts. The computational  
97 approach is accelerated using GPUs, enabling significant speedup of the geolocation and rapid execution of the  
98 model with affordable desktop computing components. The PF geolocation package was developed in Python

99 with CUDA for the accelerated sections and is available at [https://github.com/cliu3/pf\\_geolocation](https://github.com/cliu3/pf_geolocation).  
100 To the best of our knowledge, this work is the first to apply GPU-based parallelization to individual animal  
101 tracking applications and to introduce an open-source geolocation code for archival tagging based on the PF.  
102 In the following sections, we describe the specifics of the PF geolocation method and the implementation of  
103 hardware acceleration. We then present a skill assessment of the method using fixed location mooring tags  
104 and double-electronically-tagged Atlantic cod from the western Gulf of Maine. Finally we demonstrate an  
105 application of the approach by presenting geolocations of two cod.

## 106 2 Methods

### 107 2.1 The particle filter algorithm

108 Demersal fish geolocation can be described as a nonlinear filtering problem using the following state-space  
109 system (Royer et al., 2005):

$$\begin{aligned}
 \mathbf{x}^{(k)} &= f(\mathbf{x}^{(k-1)}), \\
 \mathbf{y}^{(k)} &= g(\mathbf{x}^{(k)}) + \mathbf{e}_t.
 \end{aligned}
 \tag{1}$$

110  
111 Here,  $\mathbf{x}^{(k)}$  is the state variable (geographic horizontal location of the fish) at time  $t = k\Delta t$  where  $\Delta t$  is the  
112 observation time step;  $\mathbf{y}^{(k)}$  is the observation (temperature and depth recorded by the archival tag) at the  
113 concurrent time;  $f$  is a function describing the fish’s horizontal movement;  $g$  is the observation function;  
114 and  $\mathbf{e}_t$  is the observation error (tag sensor errors). The goal is to estimate the daily location distribution of  
115 the tagged fish, i.e., the unknown state series  $\mathbf{x}$ , which requires estimating a probability distribution series  
116  $p(\mathbf{x}^{(k)}|\mathbf{y}^{(0:k)})$ , given the tag-recorded full observation series  $\mathbf{y}^{(0:k)} = \{\mathbf{y}^{(0)}, \mathbf{y}^{(1)}, \dots, \mathbf{y}^{(k)}\}$ . This is achieved  
117 using Bayesian inference:

$$\begin{aligned}
 p(\mathbf{x}^{(k)}|\mathbf{y}^{(0:k-1)}) &= \int p(\mathbf{x}^{(k)}|\mathbf{x}^{(k-1)})p(\mathbf{x}^{(k-1)}|\mathbf{y}^{(0:k-1)})d\mathbf{x}^{(k-1)}, \\
 p(\mathbf{x}^{(k)}|\mathbf{y}^{(0:k)}) &= \frac{p(\mathbf{y}^{(k)}|\mathbf{x}^{(k)})p(\mathbf{x}^{(k)}|\mathbf{y}^{(0:k-1)})}{p(\mathbf{y}^{(k)}|\mathbf{y}^{(0:k-1)})},
 \end{aligned}
 \tag{2}$$

118  
119 where the initial distribution  $p(\mathbf{x}^{(0)}|\mathbf{y}^{(0)})$  is a Gaussian distribution centered at the release location of the  
120 tagged fish, with a small standard deviation of <50 m. A PF is an algorithm for estimating a state-space

121 model in which a set of discrete samples in state space (referred to as particles) and weights indicating the  
 122 relative importance of the particles are used to approximate the predicted distribution. With respect to the  
 123 geolocation problem, each particle  $\mathbf{x}_i^{(k)}$  where  $i$  is the particle index represents the possibility of the fish's  
 124 horizontal location at discrete time  $k$ . Each particle has a corresponding weight ( $w_i^{(k)}$ ) which quantifies that  
 125 possibility. Given sufficiently large particle count,  $N$ , the particles collectively approximate the continuous  
 126 probability distribution of the fish's location.

127 A likelihood function connects the observations and the corresponding hidden states at each discrete time  
 128  $k$ . Constructing the likelihood function requires a comparison between the environmental data from archival  
 129 tagging and a regional environmental database. We used bottom water temperature, bathymetry, and tidal  
 130 elevation output from the Northeast Coastal Ocean Forecasting System (NECOFS) (Beardsley et al., 2013;  
 131 NECOFS, 2013), which was developed using the Finite-Volume Community Ocean Model (FVCOM) (Chen  
 132 et al., 2006; Cowles et al., 2008). FVCOM utilizes unstructured triangular grids which enable variation in the  
 133 horizontal resolution. In the NECOFS database, the horizontal resolution ranges from 5 km near the open  
 134 boundary to 500 m along the coast and in the vicinity of persistent tidal mixing fronts. Values of bathymetry  
 135 and bottom temperature are located at the vertices of the triangles. Previous skill assessment studies  
 136 compared the NECOFS-estimated bottom temperature with *in situ* bottom temperature measurements and  
 137 reported strong agreement (Li et al., 2017; Liu et al., 2017). The likelihood function  $L(\mathbf{x}, t)$  is derived from  
 138 a statistical comparison of environmental data from the tag and from the FVCOM database over a tolerance  
 139 interval following Le Bris et al. (2013); Liu et al. (2017); Zemeckis et al. (2017):

$$140 \quad L_{dt}(\mathbf{x}) = \int_{z-\Delta z}^{z+\Delta z} N(z; \mu_z(\mathbf{x}), \sigma_z(\mathbf{x})) dz \times \int_{T-\Delta T}^{T+\Delta T} N(T; \mu_T(\mathbf{x}), \sigma_T(\mathbf{x})) dT, \quad (3)$$

141 where  $\Delta z$  and  $\Delta T$  are the tag measurement error for depth and temperature, respectively;  $z$  and  $T$  are daily  
 142 bottom depth and the associated temperature determined from the tag data;  $N(\mu, \sigma^2)$  is a normal distribution  
 143 function of mean  $\mu$  and standard deviation  $\sigma$ , and  $\mu_z$  and  $\mu_T$  are NECOFS depth and temperature. The  
 144 standard deviations of bathymetry  $\sigma_z(\mathbf{x})$  and temperature  $\sigma_T(\mathbf{x})$  were determined using the NECOFS depth  
 145 and temperature values from the neighboring vertices of  $\mathbf{x}$  on the unstructured grid. Subsequently, likelihood  
 146 values are assigned a value of zero at locations where the possible tidal range interval estimated from NECOFS

147 does not include the range of tidal signal detected from the tag data (see Liu et al. (2017) for details). The  
 148 known recapture location was also incorporated in the likelihood function to influence movement towards this  
 149 location over the last several time steps, by confining the likelihood distribution within a circle of decreasing  
 150 radius  $R_t$  around the reported recapture location, and the radius is informed by the remaining time until  
 151 recapture, and the typical swimming speed of the species  $v_m$ , until the radius equals the reported uncertainty  
 152 radius  $r_u$  associated with the recapture location:

$$153 \quad R_t = \max(r_u, 0.5v_m(T - t)). \quad (4)$$

154 The likelihood approach is described in detail in Liu et al. (2017) and was implemented in MATLAB in the  
 155 HMM Geolocation toolbox. For the present work, the routines that construct the daily likelihood function  
 156 were converted to Python and are incorporated in the PF geolocation package.

157 There are four main steps in the PF geolocation scheme: release, prediction, update, and resampling  
 158 (Fig. 1). In the first step, the particles are initiated at the release location of the fish (Fig. 1a). This occurs  
 159 only at the beginning of the simulation. The remaining three steps are repeated each day of the geolocation  
 160 and are implemented in this study following the basic PF approach of Royer et al. (2005) and Andersen  
 161 et al. (2007) and are described in detail below.

162 The prediction step models the horizontal movement of the fish and represents behavior (see Fig. 1b).  
 163 This movement is approximated here by a random walk and was modeled directly for each particle using:

$$164 \quad \tilde{\mathbf{x}}_i^{(k)} = \mathbf{x}_i^{(k-1)} + \frac{\Delta t}{\delta t} \mathbf{R} \sqrt{2D_m \delta t}, \quad (5)$$

165 where  $i$  is the particle index,  $\Delta t = 24$  h is the time interval between observations,  $\delta t$  is the prediction sub-step,  
 166  $\mathbf{R}$  is drawn from the standard normal distribution (mean = 0; s.d. = 1) representing the process error, and  
 167  $D_m$  is a diffusion coefficient corresponding to the behavior state  $m$ . Approximating fish movement behavior  
 168 via random walk is common and estimated movement can encompass a range of possible mechanisms and  
 169 behaviors, both in geolocation applications (e.g., Sibert et al., 2003; Andersen et al., 2007; Nielsen and  
 170 Sibert, 2007; Pedersen et al., 2008, 2011a; Galuardi and Lam, 2014; Braun et al., 2018) and estimating fish

171 movements in the context of spatial stock structure (e.g., [Sibert et al., 1999](#); [Goethel et al., 2011](#); [Schwarz,](#)  
172 [2014](#)). We selected a prediction sub-step of  $\delta t = 1$  h which prevented particle displacements from exceeding  
173 the FVCOM mesh resolution along the coast. The values used for the diffusivity coefficients  $D_m$ , are species-  
174 specific and are tied to discrete behavior states. The behavior state is established based on the detection  
175 and duration of a tidal signal in the tag data on a given day following the approach used in our HMM  
176 geolocation package ([Liu et al., 2017](#); [Zemeckis et al., 2017](#)) based on the premise that a tidal signal is more  
177 discernible in low activity fish when they are sedentary on the bottom, and the diffusivity coefficient values  
178 were determined considering the typical swimming speed of the species (e.g., [Fernö et al., 2011](#)). For Atlantic  
179 cod, we allowed the behavior state  $m$  to be sedentary (low activity, 13 h tidal signal,  $D_m = 1 \text{ km}^2 \text{ day}^{-1}$ ),  
180 intermediate (moderate activity, 5 h tidal signal,  $D_m = 5 \text{ km}^2 \text{ day}^{-1}$ ), or migratory (high activity, no tidal  
181 signal,  $D_m = 10 \text{ km}^2 \text{ day}^{-1}$ ).

182 A rigorous boundary treatment was implemented to conserve the number of particles in the simulation by  
183 preventing particles from crossing onto land. To determine if a particle moved onto land during a prediction  
184 sub-step ( $\delta t$ ), a nearest-neighbor search was performed to find the two FVCOM mesh vertices nearest the  
185 new particle location. A particle that is not contained within any of the triangular cells that are connected  
186 to these two vertices was considered to have exited the domain and is subsequently reset to its prior position  
187 within the domain at the previous prediction sub-step (Fig. 2a). Conversely, a particle that is inside any  
188 of the triangular cells that are connected to the two vertices nearest the particle was considered to be in  
189 the domain and the new particle location is retained (Fig. 2b). This boundary treatment approximates a  
190 reflecting boundary condition, which is appropriate for modeling fish movements ([Sibert et al., 1999](#)). In  
191 the serial CPU version of the code, the nearest neighbor search is performed using a  $k$ -d tree algorithm  
192 ([Maneewongvatana and Mount, 1999](#)) from the SciPy Python package ([Jones et al., 2001](#)). The  $k$ -d tree is  
193 an efficient search algorithm that is optimized for the CPU. For the present work it is considerably faster  
194 than a brute-force nearest neighbor search, providing a factor of 35 speedup in benchmark testing.

195 In the update step, particle weights are first drawn from the likelihood function  $L(\mathbf{x}, t)$  evaluated at



196 particle locations  $\mathbf{x}_i^{(k)}$  and time  $t = k\Delta t$ :

$$197 \quad \tilde{w}_i^{(k)} = L(\mathbf{x}_i^{(k)}, t), \quad (6)$$

198 The particle likelihood values are computed using data that is stored discretely on the horizontal unstructured  
 199 grid of the NECOFS database. Execution of eq. (6) requires interpolating  $L(\mathbf{x}, t)$  onto each particle location.  
 200 For this work we use a routine for bilinear interpolation on triangular grids provided in the Python package  
 201 Matplotlib (Hunter, 2007). The particle weights are then normalized into the range  $0 \leq w_i^{(k)} \leq 1$

$$202 \quad w_i^{(k)} = \tilde{w}_i^{(k)} / \sum_i \tilde{w}_i^{(k)}, \quad (7)$$

203 to give the resulting posterior probability distribution at time  $t$  (Fig. 1c).

204 In the last step of the daily iteration, particles are resampled according to the particle weights ( $w_i^{(k)}$ ),  
 205 such that particles with low weights are removed and replaced by those with higher weights and particle  
 206 numbers are reordered in the new set of particles so that they are proportional to their weights (Fig. 1d).  
 207 The resampling is implemented following the approach of Labbe (2016) and is demonstrated in Fig. 3 for a  
 208 simple simulation with  $N = 10$  particles. In the first step, a cumulative density function (cdf; blue line) is  
 209 constructed using the normalized weights ( $w_j^{(k)}$ ). The cdf is then divided into  $N$  equal divisions where  $N$  is  
 210 the number of particles and a random offset is used to displace these divisions (Fig. 3, green arrows). The  
 211  $N$  particles identified by the green arrows in the cdf curve are then selected for resampling. Note that the  
 212 particle multiplicity may be greater than one. For the cdf and divisions shown in Fig. 3, the selected set  
 213 of particles is  $I = \{0, 0, 1, 3, 4, 4, 6, 8, 8, 9\}$ . The particles with multiplicity greater than unity  $\{0, 4, 8\}$  are  
 214 particles with greater weight. The particles with lower weights  $\{2, 5, 7\}$  will be re-initialized at the locations  
 215 of particles  $\{0, 4, 8\}$ , respectively. The particle position histories are transferred using the indexing array  $I$   
 216 so that particles initialized to a new location carry the location time series of the particle in that location  
 217 at time  $t$ :

$$218 \quad \mathbf{x}_i^{(j)} = \tilde{\mathbf{x}}_{I_i}^{(j)} \quad j = 0 \dots k. \quad (8)$$

219 To conduct this step we used the systematic resampling function from the package FilterPy (Labbe, 2016)  
 220 to generate an index array  $\mathbf{I}$  to the particles that have been chosen for resampling such that the numbers of  
 221 the indices to the particles before resampling equals these particles' weights:

$$222 \quad P(\mathbf{I}_i = j) = w_j. \quad (9)$$

223 After the model has been integrated from release to recapture, the estimated most probable track (MPT)  
 224 is determined. The MPT represents the track of the particle with the highest overall importance score,  
 225 defined as the product of the weight at the last time step and the sum of the weights from the first to the  
 226 second to last time steps. The index of the particle associated with the MPT is given by

$$227 \quad I_{MPT} = \arg \max_i (w_i^{(T)} \sum_{k=0}^{T-1} w_i^{(k)}) \quad (10)$$

228 where  $T$  is the last time step of the filter. In addition to the MPT, daily posterior probability distributions  
 229 of the fish are reconstructed from the horizontal distribution of particles using non-parametric kernel density  
 230 estimation. These may also be interpreted as the uncertainty distribution around the most probable track  
 231 and may be useful in interpreting the results.

232 A summary of the work flow in the present PF geolocation algorithm is provided in the table below.

1. Initialize the particles by placing them at the release location of the tagged fish (Fig. 1a).
2. FOR each day the fish is at large, do steps (a)–(c):
  - (a) Predict: move the particles horizontally using a random walk and ensure that particles do not exit the domain (Fig. 1b).
  - (b) Update: weight the particles by interpolating the observation likelihood function to the particles, and normalize the weights (Fig. 1c).
  - (c) Resample: remove particles with lower weight and replace them by those with higher weight (Fig. 1d).
3. Construct the overall probability distribution.
4. Determine the most probable track (MPT)

## 2.2 GPU parallelization

The PF geolocation algorithm was first implemented as serial CPU code. To achieve acceleration of the geolocation computation, the serial CPU code was parallelized by taking advantage of the significant computing capabilities of modern GPUs, specifically those manufactured by NVIDIA. For this we used the PyCUDA package (Klöckner et al., 2012), a Python library that provides access to the NVIDIA CUDA parallel computation platform (Nickolls et al., 2008). In the CUDA platform, memory spaces on the host (CPU) and the device (GPU) are handled separately, and data must be available in the device memory for the GPU to perform computations. Transfers of data between the host and the device are explicitly programmed and must be carefully planned because they can incur a significant overhead. Functions that are submitted to the GPU for parallel execution are referred to as kernels and are written in CUDA C, a variant of the C programming language.

Here we describe the details of the GPU-accelerated version of the PF geolocation, hereby referred to as the GPU code. We refer explicitly to the three primary steps of the PF algorithm: prediction, update, and resample (Fig. 4). During the initial benchmarking and profiling of the serial CPU code, the nearest

248 neighbor search was identified to be the most computationally intensive component. Therefore, the GPU  
249 implementation focuses primarily on the parallelization of the prediction step. In the GPU code, the  $x$  and  
250  $y$  arrays representing the horizontal coordinates of the particles are first initiated on the host at the reported  
251 release location of the fish. These arrays are then transferred to the global memory on the device. In the  
252 prediction step, random numbers required for the random walk are generated on the device using an intrinsic  
253 function provided by PyCUDA and the particle positions are updated on the device. To apply the boundary  
254 conditions, a brute force nearest neighbor search is used. This required two separate kernels, one to determine  
255 the mesh elements surrounding the two mesh vertices nearest to each particle and a second to determine if  
256 the particle resides within any of these elements. In the update step, the  $x$  and  $y$  arrays are transferred from  
257 the host to the device. The likelihood distribution  $L$  is then interpolated onto the particle positions  $(x, y)$  on  
258 the host to compute particle weights. These interpolated weights are subsequently transferred to the device.  
259 In the resampling step, the index array  $I$  is generated on the host. A kernel was written to re-arrange the  
260  $x$  and  $y$  arrays according to  $I$  on the GPU. Arrays  $x$  and  $y$  are subsequently transferred from the device to  
261 the host and stored in an array that is archived to an external data file.

## 262 **3 Validation and Performance Results**

### 263 **3.1 Tag Data and Skill Metrics**

264 Following Liu et al. (2017), two types of tag data were used for assessing the skill of the PF geolocation  
265 method. First, bottom-mooring tags which challenge the model to maintain a fixed position over time. A  
266 total of 14 Star-ODDI DSTs were moored on the bottom of different known fixed locations in Massachusetts  
267 Bay, Ipswich Bay, and Jeffreys Ledge between 2010 and 2015 (Fig. 5). The second set of tag data is derived  
268 from double-tagged Atlantic cod. During a study conducted from 2010 to 2012, individual Atlantic cod were  
269 tagged with both Star-ODDI milli-L DSTs and Vemco V16P-6H acoustic transmitters in the Spring Cod  
270 Conservation Zone (SCCZ; Fig. 5), located in northern Massachusetts Bay in the western Gulf of Maine,  
271 USA (See Dean et al. (2014); Zemeckis et al. (2014, 2017) for full tagging methods). Importantly, ten double-  
272 tagged fish were recaptured and the acoustic transmitters carried by these fish provide an independent set of

273 location estimates accurate to  $<10$  m in the SCCZ and  $<1$  km otherwise, when the tagged fish were detected  
274 within the receiving range of acoustic receiver arrays. Since the position of the animal is accurately known at  
275 these discrete locations while at-liberty, these data can be directly incorporated in the skill assessment of the  
276 geolocation method. Three error metrics were used to evaluate the model skill. The first metric (E1) is the  
277 distance between known locations and the location of the nearest modeled particle on the day of detection.  
278 The second metric (E2) is the distance between known locations and the position of the fish along the MPT  
279 on the day of detection. The third metric (E3) is whether the known location falls within the 95% credible  
280 area of the same-day probability distribution, reconstructed from all particles. The 95% credible area is  
281 defined such that the sum of the probability within the area is 95% of the total probability.

## 282 **3.2 Sensitivity to the number of particles**

283 A study was carried out to examine the influence of the particle count  $N$  on the geolocation. Seven sets of  
284 geolocation tests were conducted using particle numbers  $N$  ranging from  $2 \times 10^3$  to  $400 \times 10^3$ . For each  $N$ ,  
285 an ensemble of 30 runs were made with identical parameters. Both the E1 and E2 metrics were computed  
286 for each model run and used to evaluate convergence of the solution with  $N$ . The mean value of E1 over  
287 the ensemble decreases rapidly with increasing particle count to around  $200 \times 10^3$  particles and then begins  
288 to asymptote towards a fixed value with further increases in particle count (Fig. 6a). Statistics for the root  
289 mean square (RMS) of the E2 metric were also evaluated. The median value of the RMS of the E2 does not  
290 depend on particle count (Fig. 6b). However, the variation of the RMS of the E2 decreases with particle  
291 count up to around  $N = 200 \times 10^3$  particles and remains fairly static for  $N \geq 200 \times 10^3$ . This indicates that  
292 the geolocation reaches a particle-converged solution at  $N \sim 200 \times 10^3$  particles. Results from both the E1  
293 and E2 metrics indicate that using  $N = 200 \times 10^3$  particles is an optimal choice for both accuracy in particle  
294 filtering and computational load. This particle number was thus used in all experiments.

## 295 **3.3 Skill Assessment**

296 A skill assessment based on the E2 metric (error in the MPT) and E3 (whether known locations fall within  
297 95% credible areas) was conducted using tags from 14 mooring and 10 double-tagged cod representing 984

298 d of data. The MPT estimations of the PF geolocation method for the mooring DST locations had an RMS  
299 error of 14.95 km, and the error range was 0.01–27.53 km. The median MPT error for all mooring tags was  
300 9.71 km (Table 1), and 61.9% of the known locations fell within the 95% credible areas of the same-day  
301 posterior probability distributions. For the 10 double-tagged cod with high-resolution positions determined  
302 by acoustic telemetry detections, the RMS error of the same-day MPT estimation was 18.19 km and the  
303 median error was 6.0 km. The error range was 0.29–46.77 km (Table 1). All known locations fell within the  
304 95% credible areas of the same-day posterior probability distributions. These results indicate that the MPT  
305 determined using PF geolocation method was able to provide accurate location estimates typically on the  
306 horizontal scale of <18 km.

### 307 **3.4 Benchmarking and profiling**

308 Wall clock time for the PF geolocation code executed on serial CPU and GPU was evaluated on a high-  
309 performance computing cluster. Each node in the cluster was equipped with an Intel Core i7-950 CPU  
310 and an NVIDIA GeForce GTX 560 Ti GPU. A range of problem sizes from 12,500 to 200,000 particles  
311 was tested on data from a tagged cod with 56 d at liberty. Using the Python profiling module “cProfile”,  
312 the total runtime was decomposed into fractions spent in the prediction, update, and resampling steps.  
313 Profiling demonstrated that the majority of the computational time (>97% for all serial CPU cases, >52%  
314 for all GPU cases) was spent in the prediction step (Fig. 7a). The relationship between runtime and particle  
315 number is approximately linear for both the serial CPU and GPU implementations, and the speedup that  
316 the GPU implementation provides over the serial CPU approach increases with increasing particle count  
317  $N$ , ranging from a factor of 19.0 to 48.9 (Fig. 7b). Furthermore, in both CPU and GPU implementations,  
318 time spent in prediction and resampling steps increases as  $N$  increases, whereas the time spent in other  
319 parts is nearly constant regardless of particle counts, resulting in decreasing portion of total time (Fig. 7a).  
320 Thus, accelerating the prediction step through GPU parallelization effectively reduced overall runtime of PF  
321 geolocation.

322 A performance study of the PF geolocation method was also conducted on a wide range of NVIDIA GPUs.  
323 The set included products from four generations of hardware microarchitectures (Fermi, Kepler, Maxwell,

324 and Pascal) and both consumer (GeForce) and high-performance computing (Tesla) lines (Table 2) and  
325 represents a factor of 10 in the range of theoretical single-precision performance. These tests were conducted  
326 using 200,000 particles and tag data from the same Atlantic cod used in the CPU-GPU comparison study.  
327 CUDA Toolkit version 9.1 was used to compile kernels for all tests with the exception of those run on the  
328 legacy Fermi generation GPUs which are not supported beyond CUDA 8.0. CUDA 9.1 contains optimizations  
329 in routines used by the PF package which enable a 10% increase in performance over CUDA 8.0. Throughput,  
330 measured as the number of days at liberty that can be geolocated in an hour of compute time using 200,000  
331 particles, was used as the performance metric. The throughput on the serial CPU code was 6.4 d/h. The  
332 results suggest that performance of the model generally correlates with the theoretical performance of the  
333 hardware (GFLOPS) and that throughput is enhanced on the newer architectures with greater memory  
334 bandwidth. The greatest performance was achieved on the NVIDIA Volta V100, a powerful GPU aimed at  
335 deep learning applications with an approximate price of \$10,000 USD. Such high end hardware, however, is  
336 not necessary. The GeForce GTX 1050 is capable of geolocating 483 d of fish movement in under an hour  
337 of wall clock time. The 1050 is commonly specified in laptops and entry-level desktops and sells for ~\$100  
338 USD, considerably less than the cost of an archival storage tag. In summary, this study indicates that the  
339 GPU enables routine PF geolocations to be performed on affordable consumer-grade computers.

### 340 **3.5 Geolocation of Atlantic cod in western Gulf of Maine**

341 To demonstrate the capabilities of the PF geolocation package, we applied it to the geolocation of two  
342 Atlantic cod. For each fish, the estimated MPT and daily posterior probability distributions for each day  
343 the fish was at liberty are shown in Figs. 8 and 9. The reconstructed depth and temperature time series  
344 from the MPT are generally in good agreement with the raw tag data (Fig. 10).

345 Cod #13 was released on 11 May 2010 and recaptured on 21 Nov. 2010. During its 194 d at large, the  
346 tidal fitting algorithm identified 151 d as low activity, 32 d as moderate activity, and 11 d as high activity.  
347 The cod migrated southward from the tagging location and remained in the region between Stellwagen Bank  
348 and Cape Cod Bay for a prolonged period of time (approximately from day 20 to 120) before heading north  
349 to the location of its recapture (Fig. 8). The prolonged period of sedentary behavior was also evident in

350 the depth time series data recorded by the DST (Fig. 10a). The considerable time spent on Stellwagen  
351 Bank, away from the release and recapture locations represents information that would not be possible to  
352 determine from conventional tagging which can only inform release and recapture locations..

353 Cod #17 was released on 18 June 2010 and recaptured on 29 Aug. 2010 (72 d at large); 26, 33, and 13 days  
354 were classified as low, moderate, and high activity days, respectively. As the fish migrated northward after  
355 day 30 towards the recapture location, the posterior probability distribution exhibited a bimodal pattern,  
356 suggesting two plausible trajectories: one that extended directly northward and the other that took a more  
357 circuitous route to the east around the southern portion of Jeffreys Ledge (Fig. 9). In an ensemble of model  
358 runs, MPTs along both of these trajectories were observed, although the circuitous route was the dominant  
359 solution. The MPT from the particular model run shown in Fig. 9 follows this circuitous second trajectory.

## 360 4 Discussion

361 The open source PF geolocation package presented in this work was developed with the goal of making  
362 geolocation analyses more accessible to fisheries researchers who conduct archival tagging studies on demersal  
363 fishes. The kernel of the solver represents an implementation of the basic filter outlined in [Andersen et al.](#)  
364 [\(2007\)](#) combined with the likelihood function approach developed in our prior geolocation work ([Liu et al.](#),  
365 [2017](#)). The implementation of a rigorous boundary treatment scheme and GPU parallelization enables this  
366 software package to estimate movement in regions with complex coastline geometry and provides rapid  
367 solutions using consumer grade computer hardware readily available to researchers.

368 Results of MPT errors from PF geolocation of both mooring and double-tagging validation tests were  
369 similar to those obtained using the HMM geolocation toolbox ([Liu et al.](#), [2017](#)): RMS error for mooring tags  
370 were 14.95 km with PF and 11.07 km with HMM, while for double-tagged cod errors were 18.19 km with PF  
371 and 21.87 km with HMM. The PF geolocation exhibited slightly better overall skill in the geolocations of  
372 double-tagged fish, but with shorter runtime. For six out of ten double-tagged fish, the PF geolocation code  
373 outperformed the HMM geolocation toolbox in median geolocation error by 0.45–34.8 km. These errors were  
374 not found to decrease substantially with further increases in the number of particles in the PF or refinement  
375 of the mesh in HMM. This indicates that for this specific combination of species, tag type, and the given



376 environmental database, we may be at the limit of estimation accuracy that can be provided by state-space  
377 methods. The PF geolocation performances are similar to or better than other geolocation efforts. For  
378 example, [Hunter et al. \(2003\)](#) and [Thorsteinsson et al. \(2012\)](#) used mooring tags fixed at known locations to  
379 validate their tidal-based method and reported average error of  $15.7 \pm 3.5$  km and 18.91 km, respectively.  
380 Double-tagging studies of sharks ([Teo et al., 2004](#); [Winship et al., 2012](#)) found errors  $>0.5^\circ$  (approximately  
381 55 km). A recent HMM-based geolocation study of shark species reported median errors of 66–150 km  
382 compared to known locations with accuracy of  $<10$  km ([Braun et al., 2018](#)). Precision obtained with this  
383 methods is the among highest documented in tracking marine animals.

384 The GPU implementation of the PF geolocation package achieves up to  $75\times$  the speed of the serial  
385 CPU implementation on the affordable, consumer-grade NVIDIA GTX 1050, and up to  $266\times$  on a high-  
386 end Tesla V100 GPU. The runtime of PF geolocation of a 210 d track is well under an hour running on a  
387 typical consumer grade NVIDIA GPU with minimal specifications. This acceleration factor may be even  
388 higher if the suboptimal brute force nearest neighbor search were used in the CPU implementation rather  
389 than the optimized  $k$ -d tree algorithm. The significant acceleration achieved through GPU parallelization  
390 eliminates the requirements for costly specialized hardware. For comparison with the computation time  
391 of other geolocation applications on consumer-grade hardware, [Pedersen et al. \(2011b\)](#) reported that the  
392 finite-element geolocation method they developed takes on the order of days to estimate a 294 d track on a  
393 1.4 GHz laptop and the recently published HMM-based geolocation package HMMoce ([Braun et al., 2018](#))  
394 written in R takes nearly a full day to run a 134 d track on a quad-core personal computer. Parts of  
395 the current PF geolocation package may be further parallelized, but doing so is not likely to result in any  
396 significant improvement in performance. For example, in the current method, the prediction step is the  
397 most computationally intensive. Brute-force nearest neighbor search represents an embarrassingly parallel  
398 algorithm and the GPU implementation is much faster than the optimized  $k$ -d tree on serial CPU. The  $k$ -d  
399 tree is an optimized algorithm for serial execution that may provide  $35\times$  speedup over serial brute-force, but  
400 it is not suitable for parallel execution ([Hering, 2013](#)). Implementing this  $k$ -d tree on GPU would require a  
401 considerable undertaking with no guarantee of performance gain over the brute-force algorithm. As another  
402 example, the PF resampling in the current method is not parallelized. While parallelized PF resampling

403 algorithms have been proposed (McAlinn et al., 2016), the benefit to the overall performance would be  
404 nominal, because resampling accounts for only  $<1.2\%$  of the total runtime, and Amdahl’s Law (Amdahl,  
405 1967) predicts a maximum speedup of only  $S = 1 / (1 - \frac{1.2}{100}) \approx 1.2\%$ .

406 Most approaches to marine animal geolocation do not place emphasis on the boundary treatment. Sim-  
407 ple boundary schemes, such as masking out values on grid points representing land, may be sufficient for  
408 estimating large-scale movements of pelagic animals in which case the influence of land boundaries may  
409 be negligible, but these simple schemes cannot adequately handle the estimations of movements of coastal  
410 species in regions with complex land boundaries. In the present work, we use the unstructured triangular  
411 mesh of NECOFS database which provides significantly better resolution of the coastline compared with  
412 structured grid approaches (Chen et al., 2006). This enables us to implement a robust reflection boundary  
413 scheme in the PF geolocation package that effectively prevents particles from moving onto or crossing over  
414 land and models the fish movements more realistically. As an alternative boundary treatment, particles  
415 that move out of the domain can be eliminated. This is equivalent to an absorbing boundary condition  
416 which is not appropriate for the land-ocean boundary in modeling marine animal movements (Sibert et al.,  
417 1999). The PF geolocation package can potentially be adapted to work with other oceanographic databases  
418 that provide bathymetry and bottom temperature data for other regions. Since the boundary treatment in  
419 the PF geolocation package is dependent on the grid of the FVCOM bottom temperature data, using data  
420 from other databases requires re-implementation of the boundary treatment scheme. Bottom temperature  
421 data from many of the oceanographic databases are based on popular ocean models such as ROMS or HY-  
422 COM that use curvilinear grids, which would make the particle-based boundary treatment scheme easier to  
423 implement than the triangular grid of FVCOM (e.g., Sumner et al., 2009).

424 The PF geolocation results include the daily posterior probability distributions and the MPT. Due to the  
425 stochastic nature of the simulation, two runs with identical parameters will not produce identical results.  
426 The particle number sensitivity experiments indicate that using larger particle numbers will decrease the  
427 variability of the outcome (MPT), but there is a limit beyond which further increase in the particle count  
428 will not provide further convergence of the MPT over an ensemble of runs. As an alternative point estimate  
429 metric, maximum *a posteriori* (MAP) (Saha et al., 2009) may provide less stochastic location track estimates,

430 but the high computational complexity is likely prohibitive, especially when the particle number is large. In  
431 addition, being a single sample of all the particles, the MPT ensures that the movement model is strictly  
432 followed, making MPT a more plausible track than one estimated by the MAP. It should be noted that, as  
433 the daily posterior distributions are largely consistent across an ensemble of runs using a fixed model setup,  
434 any point estimate metric including the MPT should not be the sole information to be considered when  
435 interpreting and understanding the movements of the tagged individual.

436 The PF geolocation method uses the random walk to model individual movements, because the random  
437 walk and the equivalent Fokker-Planck diffusion model are widely accepted as appropriate for the spatial  
438 and temporal scales corresponding to tagging studies of fishes (e.g., [Sibert et al., 1999](#); [Andersen et al.,  
439 2007](#); [Pedersen et al., 2008](#); [Goethel et al., 2011](#)), and for animal movement modeling using the particle filter  
440 (e.g., [Andersen et al., 2007](#); [Tremblay et al., 2009](#); [Dowd and Joy, 2011](#); [Rakhimberdiev et al., 2015](#)). The  
441 random walk was also the choice of the movement model in many popular geolocation software packages  
442 for marine animals (e.g., `hmmgeolocation`: [Pedersen et al. 2008](#); Wildlife Computers GPE3: based on  
443 [Pedersen et al. 2011a](#); `TrackIt`: [Lam et al. 2010](#); `HMMoce`: [Braun et al. 2018](#)). Alternative movement  
444 models, such as Lévy flight, have been shown to have a negligible effect in geolocation applications compared  
445 to the random walk ([Thygesen and Nielsen, 2009](#)). Furthermore, the random walk model is effectively  
446 being used as a prior on possible moves and the estimated movement is being updated by the data very  
447 frequently, therefore the performance may be less sensitive to the choice of the movement model. Given the  
448 reasonably good performance indicated by the validation results, implementing a different movement model  
449 may unnecessarily increase the complexity of the geolocation method. In geolocating the double-tagged cod,  
450 the diffusion coefficient was estimated from the measured modal swimming speed of Atlantic cod (0.1–0.4  
451 body lengths per second, [Fernö et al. 2011](#)). Given that the lengths of the double-tagged cod are in the  
452 range of 70–110 cm, the appropriate diffusion coefficient was estimated to be  $1 \text{ km}^2 \text{ day}^{-1}$  for the low activity  
453 level, considering a small, slow fish (70 cm, 0.05 body lengths per second) and  $10 \text{ km}^2 \text{ day}^{-1}$  for the high  
454 activity level, considering a larger, faster fish (110 cm, 0.1 body lengths per second), using the equation  
455  $D = \rho v^2 / 2$ , where  $v$  is the swimming speed and  $\rho = 6 \text{ h}$  is an assumed decorrelation time ([Pedersen, 2007](#)).  
456 The PF geolocation results were found to be sensitive to values selected for the diffusion coefficients. We

457 performed the double-tagged cod validation with the increased diffusion coefficient values for low, moderate,  
458 and high activity levels of 5, 25, and 50 km<sup>2</sup> day<sup>-1</sup>, and the overall median error increased 23 km. The  
459 PF geolocation method may be further improved to be capable of estimating unknown parameters, such  
460 as the diffusion coefficient, based on a maximum likelihood approach. For example, Andersen et al. (2007)  
461 proposed using Random Walk Metropolis-Hastings combined with the PF to approximate the probability  
462 distributions of the unknown parameters. Parameter estimation for the PF is an active field of research (see  
463 e.g., Kantas et al., 2015), and developing the GPU implementation of the optimal approach is a promising  
464 future direction.

465 The main contribution of this work is the successful development of a GPU-accelerated open-source ge-  
466 olocation package using archival tagging data that can be executed on affordable computers. The source code  
467 is available on a GitHub repository at [https://github.com/cliu3/pf\\_geolocation](https://github.com/cliu3/pf_geolocation), where instructions for  
468 users and an example case that can be executed are also available. Researchers can further adapt the source  
469 code for applications to other species and regions.

## 470 Acknowledgements

471 The authors thank the Center for Scientific Computing and Visualization Research (CSCVR) at UMass  
472 Dartmouth for providing an array of hardware for benchmarking and testing. We are grateful for two  
473 anonymous reviewers who provided helpful feedback to the manuscript. Cod tagging research in the Spring  
474 Cod Conservation Zone was conducted in collaboration with the Massachusetts Division of Marine Fisheries  
475 and supported by the United States Fish and Wildlife Service through the Sportfish Restoration Act and  
476 the Massachusetts Marine Fisheries Institute. Funding for the research conducted as part of this manuscript  
477 was provided by NOAA Saltonstall-Kennedy Grant award NA15NMF4270267.

## 478 Author Contributions

479 CL designed methodology, developed the PF geolocation package, and performed analyses; DZ collected the  
480 cod DST and acoustic telemetry data; CL and GC led the writing of the manuscript. All authors contributed

481 critically to the drafts and gave final approval for publication.

## 482 **References**

483 Amdahl, G., 1967. Validity of the single processor approach to achieving large-scale computing capabilities,  
484 in: Proceedings of the American Federation of Information Processing Societies, volume 30, 483–485, URL  
485 <http://doi.acm.org/10.1145/1465482.1465560>.

486 Andersen, K., Nielsen, A., Thygesen, U., Hinrichsen, H.-H., Neuenfeldt, S., 2007. Using the particle fil-  
487 ter to geolocate Atlantic cod (*Gadus morhua*) in the Baltic Sea, with special emphasis on determining  
488 uncertainty, Can. J. Fish. Aquat. Sci. 64, 618–627, doi:10.1139/f07-037.

489 Beardsley, R. C., Chen, C., Xu, Q., 2013. Coastal flooding in Scituate (MA): A FVCOM study of the 27  
490 December 2010 nor'easter, J. Geophys. Res.-Oceans 118 (11), 6030–6045, doi:10.1002/2013JC008862, URL  
491 <http://onlinelibrary.wiley.com/doi/10.1002/2013JC008862/abstract>.

492 Braun, C. D., Galuardi, B., Thorrold, S. R., 2018. HMMoce: An R package for improved geolocation of  
493 archival-tagged fishes using a hidden Markov method, Methods in Ecology and Evolution doi:10.1111/  
494 2041-210X.12959.

495 Brickman, D., Thorsteinsson, V., 2008. Geolocation of Icelandic cod from DST data using a modified particle  
496 filter method, ICES CM 2008/P.09 .

497 Chen, C., Beardsley, R. C., Cowles, G., 2006. An Unstructured Grid, Finite-Volume Coastal Ocean Model  
498 (FVCOM) System, Oceanography 19 (1), 78, URL [http://www.tos.org/oceanography/archive/19-1\\_](http://www.tos.org/oceanography/archive/19-1_chen.html)  
499 [chen.html](http://www.tos.org/oceanography/archive/19-1_chen.html).

500 Coleman, K. E., 2015. Understanding the winter flounder (*Pseudopleuronectes americanus*) southern New  
501 England/Mid-Atlantic stock through historical trawl surveys and monitoring cross continental shelf move-  
502 ment, MS thesis, Rutgers University, New Brunswick, NJ.

503 Cowles, G. W., Lentz, S. J., Chen, C., Xu, Q., Beardsley, R. C., 2008. Comparison of observed and  
504 model-computed low frequency circulation and hydrography on the New England Shelf, J. Geophys. Res.-

505 Oceans 113 (C9), C09015, doi:10.1029/2007JC004394, URL <http://www.agu.org/pubs/crossref/2008/>  
506 [2007JC004394.shtml](http://www.agu.org/pubs/crossref/2008/2007JC004394.shtml).

507 Dean, M. J., Hoffman, W. S., Zemeckis, D. R., Armstrong, M. P., 2014. Fine-scale diel and gender-  
508 based patterns in behaviour of Atlantic cod (*Gadus morhua*) on a spawning ground in the Western  
509 Gulf of Maine, ICES J. Mar. Sci. 71 (6), 1474–1489, doi:10.1093/icesjms/fsu040, URL [http://icesjms.](http://icesjms.oxfordjournals.org/cgi/doi/10.1093/icesjms/fsu040)  
510 [oxfordjournals.org/cgi/doi/10.1093/icesjms/fsu040](http://icesjms.oxfordjournals.org/cgi/doi/10.1093/icesjms/fsu040).

511 Dowd, M., Joy, R., 2011. Estimating behavioral parameters in animal movement models using a state-  
512 augmented particle filter, Ecology 92 (3), 568–575, doi:10.1890/10-0611.1.

513 Fernö, A., Jørgensen, T., Løkkeborg, S., Winger, P. D., 2011. Variable swimming speeds in individual  
514 Atlantic cod (*Gadus morhua* L.) determined by high-resolution acoustic tracking, Marine Biology Re-  
515 search 7 (3), 310–313, doi:10.1080/17451000.2010.492223, URL [http://www.tandfonline.com/doi/abs/](http://www.tandfonline.com/doi/abs/10.1080/17451000.2010.492223)  
516 [10.1080/17451000.2010.492223](http://www.tandfonline.com/doi/abs/10.1080/17451000.2010.492223).

517 Galuardi, B., Lam, C. H. T., 2014. Telemetry Analysis of Highly Migratory Species, in: Cadrin, S. X., Kerr,  
518 L. A., Mariani, S. (Eds.), Stock Identification Methods (Second Edition), Academic Press, San Diego,  
519 447–476.

520 Goethel, D. R., Quinn, T. J., Cadrin, S. X., 2011. Incorporating spatial structure in stock assessment:  
521 movement modeling in marine fish population dynamics, Rev. Fish. Sci. 19 (2), 119–136, doi:10.1080/  
522 10641262.2011.557451.

523 Goodrum, M. A., Trotter, M. J., Aksel, A., Acton, S. T., Skadron, K., 2011. Parallelization of Particle  
524 Filter Algorithms, in: Varbanescu, A. L., Molnos, A., Nieuwpoort, R. v. (Eds.), Computer Architecture,  
525 Springer Berlin Heidelberg, no. 6161 in Lecture Notes in Computer Science, 139–149, URL [http://link.](http://link.springer.com/silk.library.umass.edu/chapter/10.1007/978-3-642-24322-6_12)  
526 [springer.com/silk.library.umass.edu/chapter/10.1007/978-3-642-24322-6\\_12](http://link.springer.com/silk.library.umass.edu/chapter/10.1007/978-3-642-24322-6_12).

527 Gustafsson, F., Gunnarsson, F., Bergman, N., Forssell, U., Jansson, J., Karlsson, R., Nordlund, P. J., 2002.  
528 Particle filters for positioning, navigation, and tracking, IEEE Transactions on Signal Processing 50 (2),  
529 425–437, doi:10.1109/78.978396.

530 Hendeby, G., Karlsson, R., Gustafsson, F., 2010. Particle Filtering: The Need for Speed, EURASIP Journal  
531 on Advances in Signal Processing 2010, 22:1–22:9, doi:10.1155/2010/181403, URL [http://dx.doi.org/  
532 10.1155/2010/181403](http://dx.doi.org/10.1155/2010/181403).

533 Hering, T., 2013. Parallel Execution of kNN-Queries on in-memory KD Trees, in: Proc. of 15th GI Symposium  
534 on Business, Technology & Web (BTW'13), Magdeburg, Germany, 257–266, URL [http://cs.emis.de/  
535 LNI/Proceedings/Proceedings216/257.pdf](http://cs.emis.de/LNI/Proceedings/Proceedings216/257.pdf).

536 Hunter, E., Aldridge, J. N., Metcalfe, J. D., Arnold, G. P., 2003. Geolocation of free-ranging fish on the  
537 European continental shelf as determined from environmental variables - I. Tidal location method, Marine  
538 Biology 142 (3), 601–609, doi:10.1007/s00227-0984-5. WOS:000182387900021.

539 Hunter, J. D., 2007. Matplotlib: A 2d graphics environment, Computing In Science & Engineering 9 (3),  
540 90–95, doi:10.1109/MCSE.2007.55.

541 Hussey, N. E., Kessel, S. T., Aarestrup, K., Cooke, S. J., Cowley, P. D., Fisk, A. T., Harcourt, R. G., Holland,  
542 K. N., Iverson, S. J., Kocik, J. F., Flemming, J. E. M., Whoriskey, F. G., 2015. Aquatic animal telemetry:  
543 A panoramic window into the underwater world, Science 348 (6240), 1255642, doi:10.1126/science.1255642,  
544 URL <http://science.sciencemag.org/content/348/6240/1255642>.

545 Jones, E., Oliphant, T., Peterson, P., others, 2001. SciPy: Open source scientific tools for Python, URL  
546 <http://www.scipy.org>. <http://www.scipy.org>. [Online; accessed 2018-01-11].

547 Jonsen, I., Basson, M., Bestley, S., Bravington, M., Patterson, T., Pedersen, M., Thomson, R., Thygesen, U.,  
548 Wotherspoon, S., 2013. State-space models for bio-loggers: A methodological road map, Deep Sea Res. Part  
549 II 88–89, 34–46, doi:10.1016/j.dsr2.2012.07.008, URL [http://linkinghub.elsevier.com/retrieve/pii/  
550 S096706451200094X](http://linkinghub.elsevier.com/retrieve/pii/S096706451200094X).

551 Kantas, N., Doucet, A., Singh, S. S., Maciejowski, J., Chopin, N., 2015. On particle methods for parameter  
552 estimation in state-space models, Statistical Science 30 (3), 328–351, doi:10.1214/14-STS511, URL [https:  
553 //projecteuclid.org/euclid.ss/1439220716](https://projecteuclid.org/euclid.ss/1439220716).

554 Klöckner, A., Pinto, N., Lee, Y., Catanzaro, B., Ivanov, P., Fasih, A., 2012. PyCUDA and PyOpenCL:  
555 A Scripting-Based Approach to GPU Run-Time Code Generation, *Parallel Computing* 38 (3), 157–174,  
556 doi:10.1016/j.parco.2011.09.001.

557 Labbe, R. R., 2016. Kalman and bayesian filters in python, URL [https://github.com/  
558 rllabbe/Kalman-and-Bayesian-Filters-in-Python/](https://github.com/rllabbe/Kalman-and-Bayesian-Filters-in-Python/). Available at [https://github.com/rllabbe/  
559 Kalman-and-Bayesian-Filters-in-Python/](https://github.com/rllabbe/<br/>559 Kalman-and-Bayesian-Filters-in-Python/). Accessed 2018-01-07.

560 Lam, C. H., Nielsen, A., Sibert, J. R., 2010. Incorporating sea-surface temperature to the light-based geolo-  
561 cation model TrackIt, *Marine Ecology Progress Series* 419, 71–84, doi:10.3354/meps08862.

562 Le Bris, A., Fréchet, A., Wroblewski, J. S., 2013. Supplementing electronic tagging with conventional tagging  
563 to redesign fishery closed areas, *Fish. Res.* 148, 106–116, doi:10.1016/j.fishres.2013.08.013, URL [http:  
564 //linkinghub.elsevier.com/retrieve/pii/S0165783613002063](http://linkinghub.elsevier.com/retrieve/pii/S0165783613002063).

565 Li, B., Tanaka, K. R., Chen, Y., Brady, D. C., Thomas, A. C., 2017. Assessing the quality of bottom water  
566 temperatures from the Finite-Volume Community Ocean Model (FVCOM) in the Northwest Atlantic Shelf  
567 region, *Journal of Marine Systems* doi:10.1016/j.jmarsys.2017.04.001, URL [http://www.sciencedirect.  
568 com/science/article/pii/S092479631630358X](http://www.sciencedirect.com/science/article/pii/S092479631630358X).

569 Liu, C., Cowles, G. W., Zemeckis, D. R., Cadrin, S. X., Dean, M. J., 2017. Validation of a hidden  
570 Markov model for the geolocation of Atlantic cod, *Canadian Journal of Fisheries and Aquatic Sci-*  
571 *ences* 74 (11), 1862–1877, doi:10.1139/cjfas-2016-0376, URL [http://www.nrcresearchpress.com/doi/  
572 10.1139/cjfas-2016-0376](http://www.nrcresearchpress.com/doi/10.1139/cjfas-2016-0376).

573 Maneewongvatana, S., Mount, D. M., 1999. It’s okay to be skinny, if your friends are fat, in: *Center for*  
574 *Geometric Computing 4th Annual Workshop on Computational Geometry*, URL [https://cs.umd.edu/  
575 ~mount/Papers/cgc99-smpack.pdf](https://cs.umd.edu/~mount/Papers/cgc99-smpack.pdf).

576 McAlinn, K., Katsura, H., Nakatsuma, T., 2016. Fully Parallel Particle Learning for GPGPUs and Other  
577 Parallel Devices, arXiv preprint arXiv:1212.1639 URL <http://arxiv.org/abs/1212.1639>.



578 Metcalfe, J. D., Arnold, G. P., 1997. Tracking fish with electronic tags, *Nature* 387 (6634), 665–666, doi:  
579 10.1038/42622.

580 NECOFS, 2013. Northeast Coastal Ocean Forecasting System (NECOFS) Main Portal [http://fvcom.  
581 smast.umassd.edu/necofs/](http://fvcom.smast.umassd.edu/necofs/). Accessed: 2018-01-08.

582 Nickolls, J., Buck, I., Garland, M., Skadron, K., 2008. Scalable Parallel Programming with CUDA, *Queue*  
583 6 (2), 40–53, doi:10.1145/1365490.1365500, URL <http://doi.acm.org/10.1145/1365490.1365500>.

584 Nielsen, A., 2004. Estimating fish movement, Ph.D. thesis, Royal Veterinary and Agricultural University,  
585 URL [http://geolocation.umassd.wikispaces.net/file/view/Nielson\\_2004.pdf](http://geolocation.umassd.wikispaces.net/file/view/Nielson_2004.pdf).

586 Nielsen, A., Sibert, J. R., 2007. State–space model for light-based tracking of marine animals, *Canadian*  
587 *Journal of Fisheries and Aquatic Sciences* 64 (8), 1055–1068, doi:10.1139/f07-064.

588 Patterson, T., Thomas, L., Wilcox, C., Ovaskainen, O., Matthiopoulos, J., 2008. State–space models of  
589 individual animal movement, *Trends in Ecology & Evolution* 23 (2), 87–94, doi:10.1016/j.tree.2007.10.009.

590 Pedersen, M., Berg, C., Thygesen, U., Nielsen, A., Madsen, H., 2011a. Estimation methods for nonlinear  
591 state-space models in ecology, *Ecol. Model.* 222 (8), 1394–1400, doi:10.1016/j.ecolmodel.2011.01.007, URL  
592 <http://linkinghub.elsevier.com/retrieve/pii/S0304380011000299>.

593 Pedersen, M., Thygesen, U., Madsen, H., 2011b. Nonlinear tracking in a diffusion process with a Bayesian  
594 filter and the finite element method, *Comput Stat Data Anal* 55 (1), 280–290, doi:10.1016/j.csda.2010.04.  
595 018, URL <http://linkinghub.elsevier.com/retrieve/pii/S0167947310001635>.

596 Pedersen, M. W., 2007. Hidden Markov models for geolocation of fish, Master’s thesis, Technical University  
597 of Denmark, DTU, DK-2800 Kgs. Lyngby, Denmark, URL <http://etd.dtu.dk/thesis/200722/>.

598 Pedersen, M. W., Righton, D., Thygesen, U. H., Andersen, K. H., Madsen, H., 2008. Geolocation of North  
599 Sea cod (*Gadus morhua*) using hidden Markov models and behavioural switching, *Can. J. Fish. Aquat.*  
600 *Sci.* 65 (11), 2367–2377.

601 Rakhimberdiev, E., Winkler, D. W., Bridge, E., Seavy, N. E., Sheldon, D., Piersma, T., Saveliev, A., 2015.  
602 A hidden Markov model for reconstructing animal paths from solar geolocation loggers using templates  
603 for light intensity, *Movement Ecology* 3 (1), 25, doi:10.1186/s40462-015-0062-5.

604 Righton, D., Mills, C., 2008. Reconstructing the movements of free-ranging demersal fish in the North Sea: a  
605 data-matching and simulation method, *Mar. Biol.* 153 (4), 507–521, doi:10.1007/s00227-007-0818-6, URL  
606 <http://dx.doi.org/10.1007/s00227-007-0818-6>.

607 Royer, F., Fromentin, J.-M., Gaspar, P., 2005. A state-space model to derive bluefin tuna movement and  
608 habitat from archival tags, *Oikos* 109 (3), 473–484, doi:10.1111/j.0030-1299.2005.13777.x, URL <http://onlinelibrary.wiley.com/doi/10.1111/j.0030-1299.2005.13777.x/abstract>.

609

610 Saha, S., Boers, Y., Driessen, H., Mandal, P. K., Bagchi, A., 2009. Particle based MAP state estimation: A  
611 comparison, in: 2009 12th International Conference on Information Fusion, 278–283.

612 Schwarz, C. J., 2014. Estimation of movement from tagging data, in: Cadrin, S. X., Kerr, L. A., Mariani, S.  
613 (Eds.), *Stock Identification Methods (Second Edition)*, Academic Press, San Diego, 429–446.

614 Sibert, J. R., Hampton, J., Fournier, D. A., Bills, P. J., 1999. An advection–diffusion–reaction model for the  
615 estimation of fish movement parameters from tagging data, with application to skipjack tuna (*Katsuwonus*  
616 *pelamis*), *Canadian Journal of Fisheries and Aquatic Sciences* 56 (6), 925–938, doi:10.1139/f99-017, URL  
617 <http://www.nrcresearchpress.com/doi/abs/10.1139/f99-017>.

618 Sibert, J. R., Musyl, M. K., Brill, R. W., 2003. Horizontal movements of bigeye tuna (*Thunnus Obesus*)  
619 near Hawaii determined by Kalman filter analysis of archival tagging data, *Fisheries Oceanography* 12 (3),  
620 141–151, doi:10.1046/j.1365-2419.2003.00228.x.

621 Sumner, M. D., Wotherspoon, S. J., Hindell, M. A., 2009. Bayesian Estimation of Animal Movement from  
622 Archival and Satellite Tags, *PLoS One* 4 (10), e7324, doi:10.1371/journal.pone.0007324, URL [http://dx.](http://dx.doi.org/10.1371/journal.pone.0007324)  
623 [doi.org/10.1371/journal.pone.0007324](http://dx.doi.org/10.1371/journal.pone.0007324).

624 Teo, S. L., Boustany, A., Blackwell, S., Walli, A., Weng, K. C., Block, B. A., 2004. Validation of ge-  
625 olocation estimates based on light level and sea surface temperature from electronic tags, *Mar. Ecol.*

626 Prog. Ser. 283, 81–98, URL [http://www.soest.hawaii.edu/oceanography/faculty/kweng/Teo2004\\_](http://www.soest.hawaii.edu/oceanography/faculty/kweng/Teo2004_)  
627 [geolocation.pdf](http://www.soest.hawaii.edu/oceanography/faculty/kweng/Teo2004_geolocation.pdf).

628 Thorsteinsson, V., Pálsson, O. K., Tómasson, G. G., Jónsdóttir, I. G., Pampoulie, C., 2012. Consistency  
629 in the behaviour types of the Atlantic cod: repeatability, timing of migration and geo-location, Mar.  
630 Ecol. Prog. Ser. 462, 251–260, doi:10.3354/meps09852, URL [http://www.int-res.com/abstracts/meps/  
631 v462/p251-260/](http://www.int-res.com/abstracts/meps/v462/p251-260/).

632 Thygesen, U. H., Nielsen, A., 2009. Lessons from a Prototype Geolocation Problem, in: Nielsen, J. L., Ar-  
633 rizabalaga, H., Fragoso, N., Hobday, A., Lutcavage, M., Sibert, J. (Eds.), Tagging and Tracking of Marine  
634 Animals with Electronic Devices, Springer Netherlands, no. 9 in Reviews: Methods and Technologies in  
635 Fish Biology and Fisheries, 257–276.

636 Thygesen, U. H., Pedersen, M. W., Madsen, H., 2009. Geolocating Fish Using Hidden Markov Models  
637 and Data Storage Tags, in: Nielsen, J. L., Arrizabalaga, H., Fragoso, N., Hobday, A., Lutcavage, M.,  
638 Sibert, J. (Eds.), Tagging and Tracking of Marine Animals with Electronic Devices, Springer Netherlands,  
639 no. 9 in Reviews: Methods and Technologies in Fish Biology and Fisheries, 277–293, URL [http://link.  
640 springer.com/silk.library.umass.edu/chapter/10.1007/978-1-4020-9640-2\\_17](http://link.springer.com/silk/library.umass.edu/chapter/10.1007/978-1-4020-9640-2_17).

641 Tremblay, Y., Robinson, P. W., Costa, D. P., 2009. A Parsimonious Approach to Modeling Animal Movement  
642 Data, PLoS ONE 4 (3), e4711, doi:10.1371/journal.pone.0004711, URL [http://dx.doi.org/10.1371/  
643 journal.pone.0004711](http://dx.doi.org/10.1371/journal.pone.0004711).

644 Vuduc, R., Choi, J., 2013. A Brief History and Introduction to GPGPU, in: Modern Accelerator Technologies  
645 for Geographic Information Science, Springer, Boston, MA, 9–23, doi:10.1007/978-1-4614-8745-6\_2, URL  
646 [https://link.springer.com/chapter/10.1007/978-1-4614-8745-6\\_2](https://link.springer.com/chapter/10.1007/978-1-4614-8745-6_2).

647 Winship, A. J., Jorgensen, S. J., Shaffer, S. A., Jonsen, I. D., Robinson, P. W., Costa, D. P., Block, B. A.,  
648 2012. State-space framework for estimating measurement error from double-tagging telemetry experiments,  
649 Methods Ecol. Evol. 3 (2), 291–302, doi:10.1111/j.2041-210X.2011.00161.x.

650 Woillez, M., Fablet, R., Ngo, T.-T., Lalire, M., Lazure, P., de Pontual, H., 2016. A HMM-based model

651 to geolocate pelagic fish from high-resolution individual temperature and depth histories: European sea  
652 bass as a case study, *Ecological Modelling* 321, 10–22, doi:10.1016/j.ecolmodel.2015.10.024, URL [http:  
653 //www.sciencedirect.com/science/article/pii/S0304380015005098](http://www.sciencedirect.com/science/article/pii/S0304380015005098).

654 Zemeckis, D., Liu, C., Cowles, G., Dean, M., Hoffman, W., Martins, D., Cadrin, S., 2017. Seasonal movements  
655 and connectivity of an Atlantic cod (*Gadus morhua*) spawning component in the western Gulf of Maine,  
656 *ICES Journal of Marine Science* 74 (6), 1780–1796, doi:10.1093/icesjms/fsw190.

657 Zemeckis, D. R., Hoffman, W. S., Dean, M. J., Armstrong, M. P., Cadrin, S. X., 2014. Spawning site  
658 fidelity by Atlantic cod (*Gadus morhua*) in the Gulf of Maine: implications for population structure  
659 and rebuilding, *ICES J. Mar. Sci.* 71 (6), 1356–1365, doi:10.1093/icesjms/fsu117, URL [http://icesjms.  
660 oxfordjournals.org/cgi/doi/10.1093/icesjms/fsu117](http://icesjms.oxfordjournals.org/cgi/doi/10.1093/icesjms/fsu117).

661 **List of Figures**

662 1 Demonstration of the steps of the particle filter: release, prediction, update, and resample.  
663 This is an example of cod in the Gulf of Maine. Color indicates values of the daily likelihood  
664 distribution  $L_{dt}$ . . . . . 31

665 2 Boundary treatment of the particles during the prediction step. After the tentative movement  
666 established by the horizontal random walk (black particles), each particle is then classified  
667 as being outside or inside the domain. (a) A particle not found in all of the triangular cells  
668 (red triangles) surrounding the two nearest mesh vertices (blue dots) is characterized as being  
669 outside of the domain, and is subsequently restored to the location where it resided prior to  
670 the step. (b) A particle found in any of the triangular cells (green triangles) surrounding the  
671 two nearest mesh vertices (blue circles) is characterized as being inside of the domain and is  
672 allowed to remain in the new location. . . . . 32

673 3 Schematic plot of the resampling process for  $N = 10$  particles. The blue line is the cumulative  
674 density function (cdf), and the vertical axis is the particle index. Green arrows represent the  
675 equal divisions to determine which particles are sampled. . . . . 33

676 4 Flow chart of the parallel particle filter geolocation on graphics processing units (GPUs). . . 34

677 5 Map of western Gulf of Maine showing the Cape Cod Bay, Stellwagen Bank, Jeffreys Ledge,  
678 and the Spring Cod Conservation Zone (SCCZ) as the red rectangle. Selective isobaths of 50  
679 m, 100 m, and 200 m are also shown as lines of decreasing shades of gray with greater depth. 35

680 6 (a) Error bar plot of the distance between the nearest modeled particle and the associated  
681 acoustic location, showing the mean values (solid dots) and range (whiskers). (b) Box plot  
682 of RMS Error of the most probable track (MPT) in relation to the number of particles used  
683 in a particle filter geolocation run, over 30 model runs for each particle number, showing  
684 median values (thick black horizontal line), 25% and 75% percentile values (box outline),  
685 outliers (hollow circle), and the highest and lowest value within 1.5 times the interquartile  
686 range (whiskers). . . . . 36

|     |    |   |    |
|-----|----|---|----|
| 687 | 7  | Comparison of the time percentage for each step (a) for the PF geolocation between serial CPU (left bars) and GPU (right bars) and total run time and speed-up factors (b). . . . .   | 37 |
| 688 |    |   |    |
| 689 | 8  | Progression of the daily posterior distribution (color rendering) and the most probable track (MPT, black line) for cod #13. Black cross: release location, black triangle: reported recapture location, red triangle: simulated recapture location. . . . .                              | 38 |
| 690 |    |   |    |
| 691 |    |   |    |
| 692 | 9  | Progression of the daily posterior distribution (color rendering) and the most probable track (MPT, black line) for cod #17. Black cross: release location, black triangle: reported recapture location, red triangle: simulated recapture location. . . . .                              | 39 |
| 693 |    |   |    |
| 694 |    |   |    |
| 695 | 10 | Comparison of the raw depth and temperature time series data recorded by the data storage tags (DSTs; blue line) and the daily depth and temperature data reconstructed from environmental database along the most probable track (MPT; orange line) for (a) cod #13 and (b) #17. . . . . | 40 |
| 696 |    |   |    |
| 697 |    |   |    |
| 698 |    |   |    |

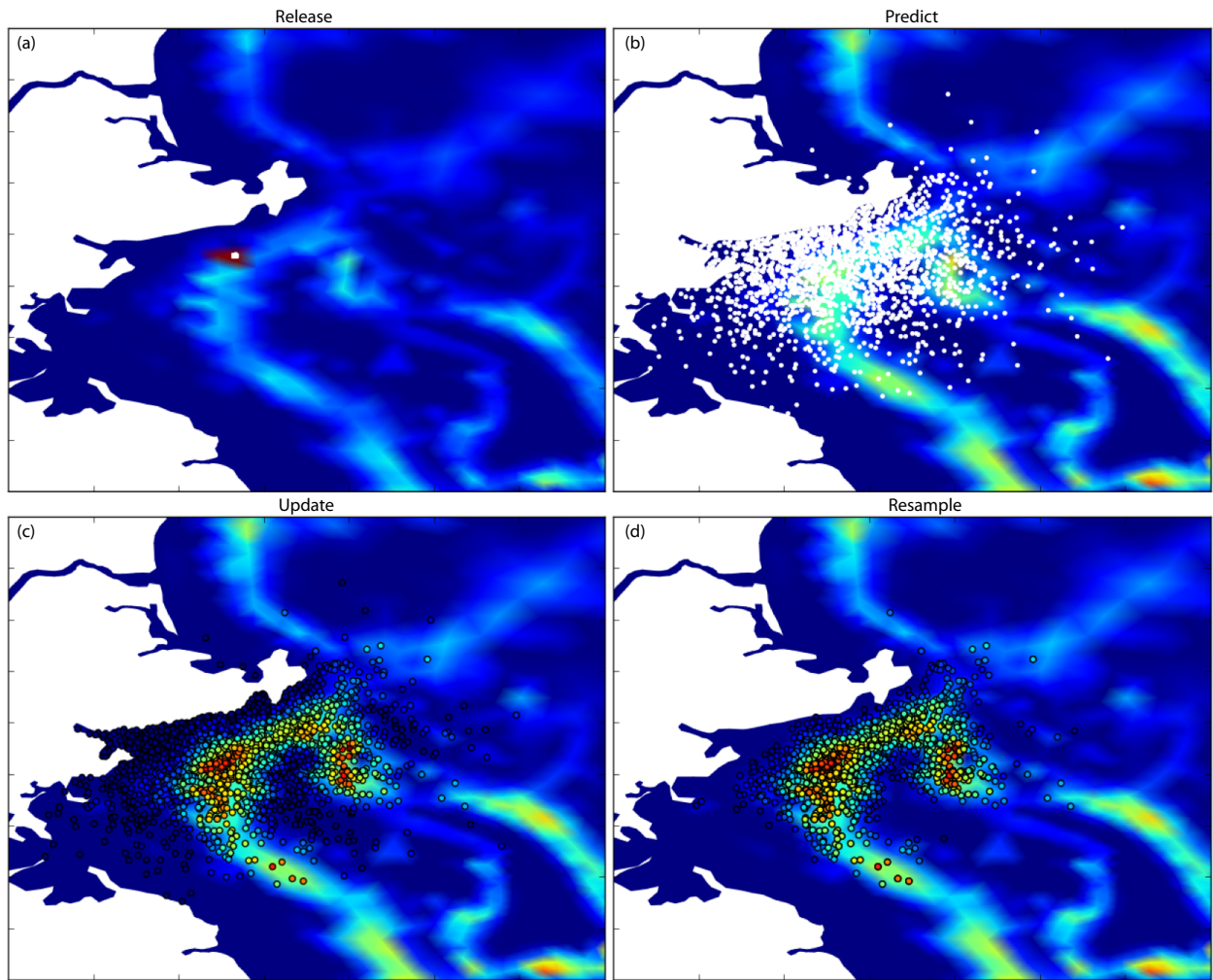


Figure 1: Demonstration of the steps of the particle filter: release, prediction, update, and resample. This is an example of cod in the Gulf of Maine. Color indicates values of the daily likelihood distribution  $L_{dt}$ .

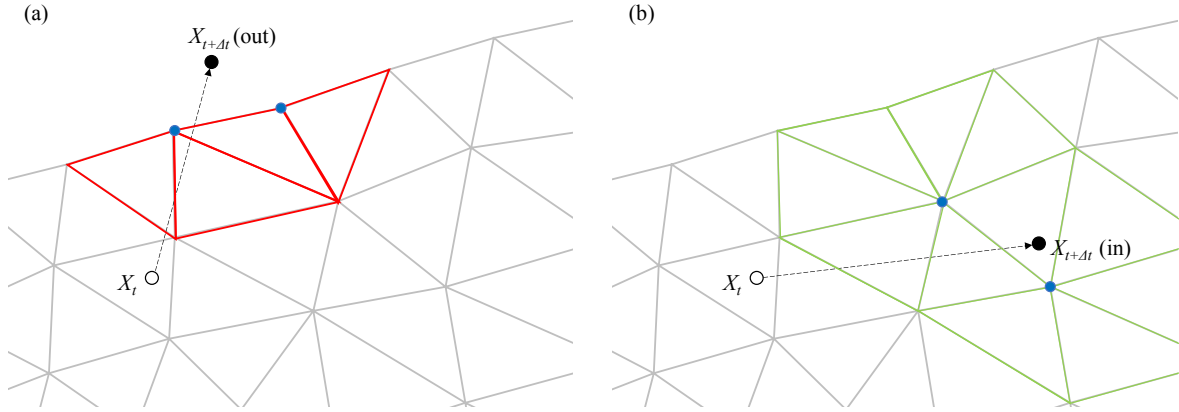


Figure 2: Boundary treatment of the particles during the prediction step. After the tentative movement established by the horizontal random walk (black particles), each particle is then classified as being outside or inside the domain. (a) A particle not found in all of the triangular cells (red triangles) surrounding the two nearest mesh vertices (blue dots) is characterized as being outside of the domain, and is subsequently restored to the location where it resided prior to the step. (b) A particle found in any of the triangular cells (green triangles) surrounding the two nearest mesh vertices (blue circles) is characterized as being inside of the domain and is allowed to remain in the new location.



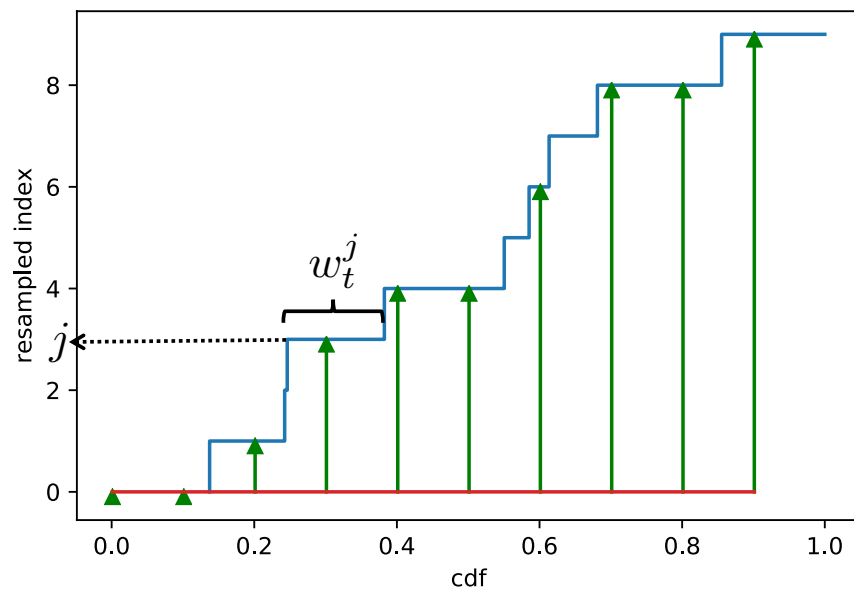


Figure 3: Schematic plot of the resampling process for  $N = 10$  particles. The blue line is the cumulative density function (cdf), and the vertical axis is the particle index. Green arrows represent the equal divisions to determine which particles are sampled.

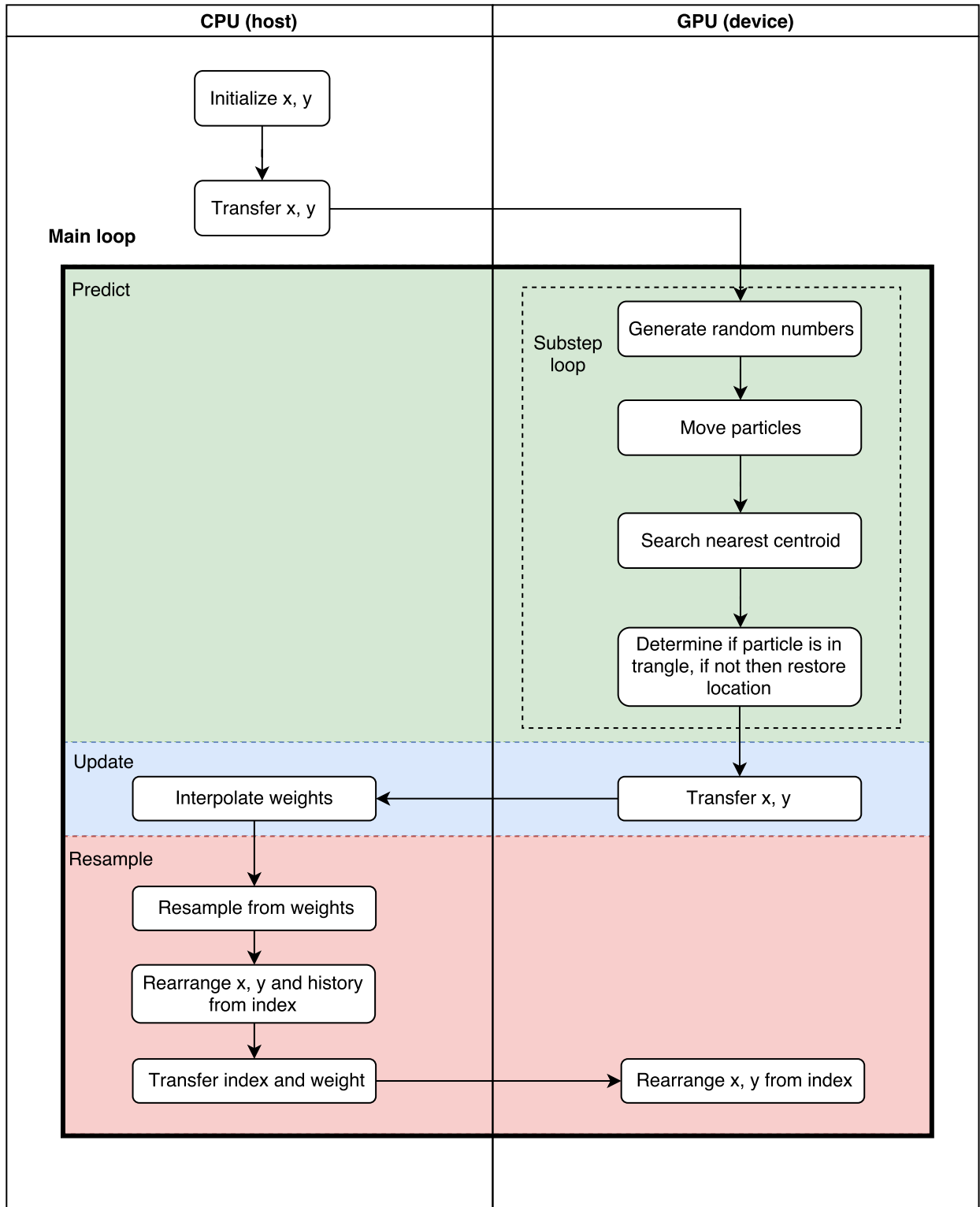


Figure 4: Flow chart of the parallel particle filter geolocation on graphics processing units (GPUs).

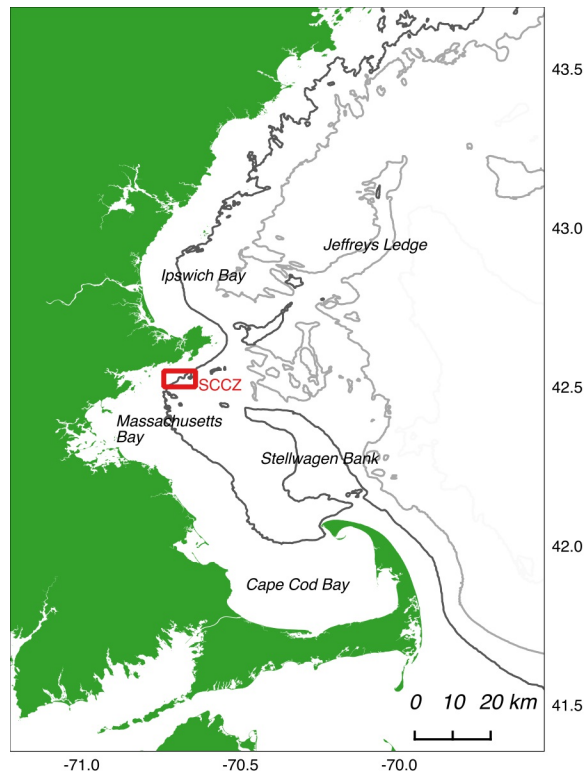
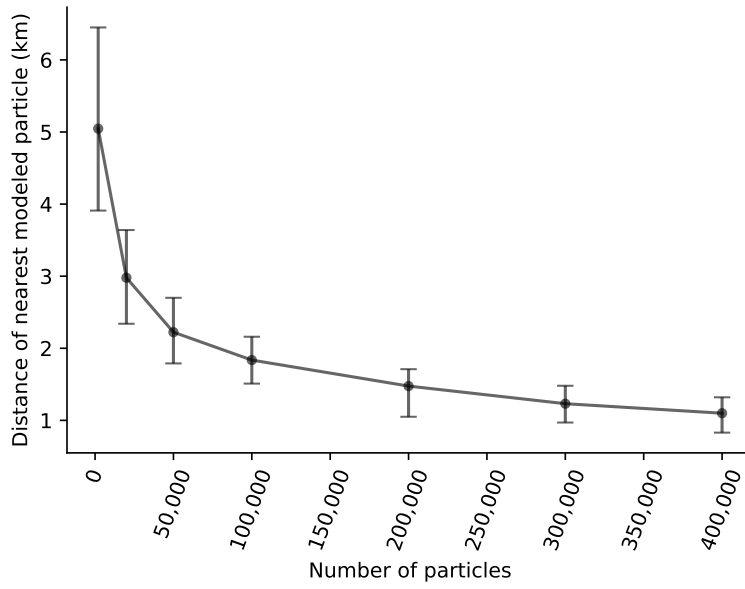
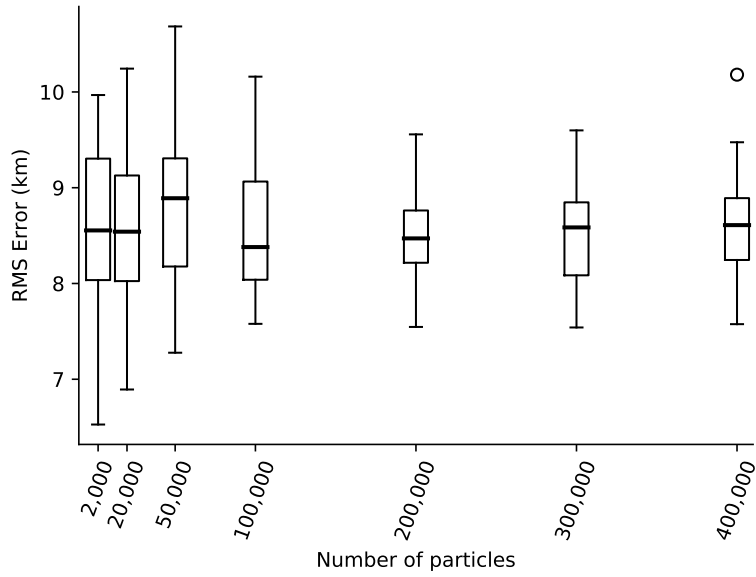


Figure 5: Map of western Gulf of Maine showing the Cape Cod Bay, Stellwagen Bank, Jeffreys Ledge, and the Spring Cod Conservation Zone (SCCZ) as the red rectangle. Selective isobaths of 50 m, 100 m, and 200 m are also shown as lines of decreasing shades of gray with greater depth.

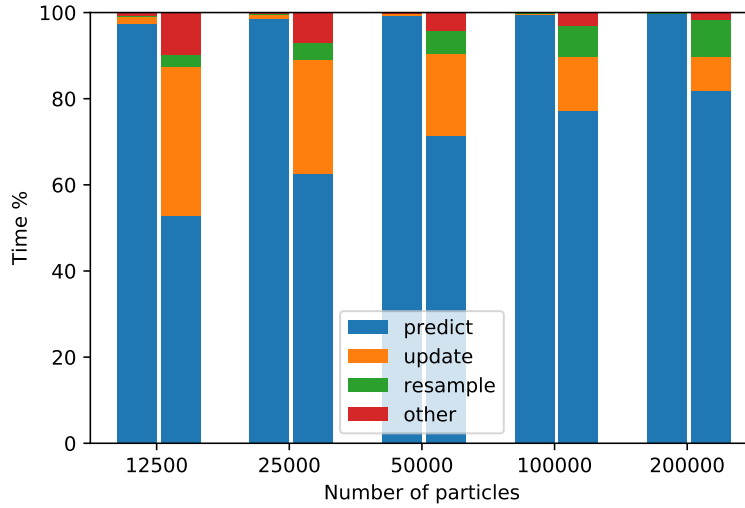


(a)

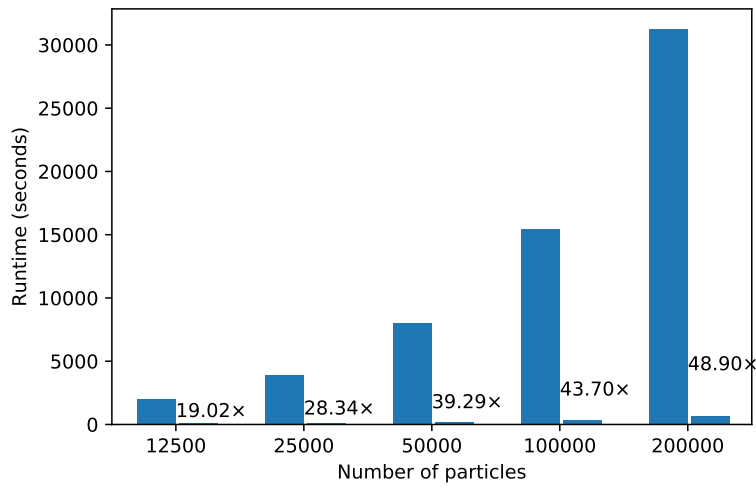


(b)

Figure 6: (a) Error bar plot of the distance between the nearest modeled particle and the associated acoustic location, showing the mean values (solid dots) and range (whiskers). (b) Box plot of RMS Error of the most probable track (MPT) in relation to the number of particles used in a particle filter geolocation run, over 30 model runs for each particle number, showing median values (thick black horizontal line), 25% and 75% percentile values (box outline), outliers (hollow circle), and the highest and lowest value within 1.5 times the interquartile range (whiskers).



(a)



(b)

Figure 7: Comparison of the time percentage for each step (a) for the PF geolocation between serial CPU (left bars) and GPU (right bars) and total run time and speed-up factors (b).

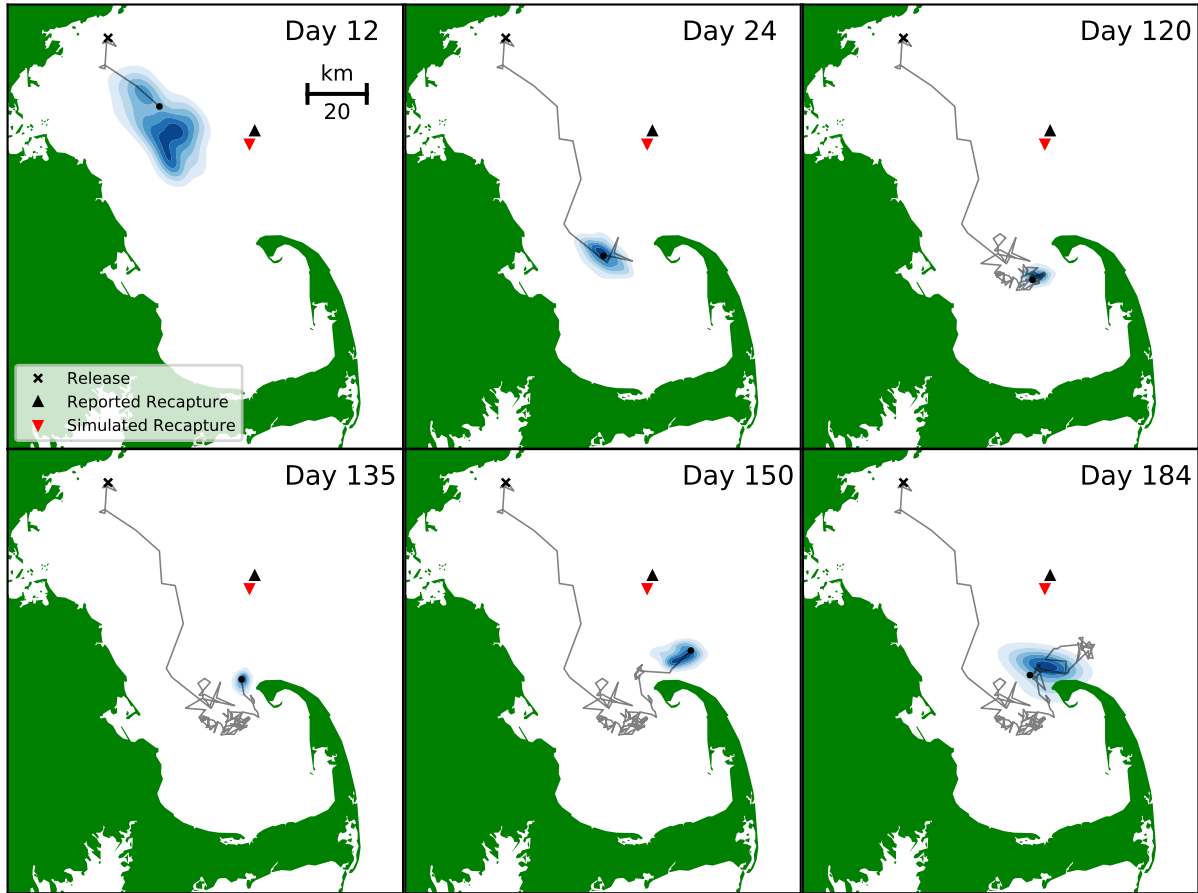


Figure 8: Progression of the daily posterior distribution (color rendering) and the most probable track (MPT, black line) for cod #13. Black cross: release location, black triangle: reported recapture location, red triangle: simulated recapture location.

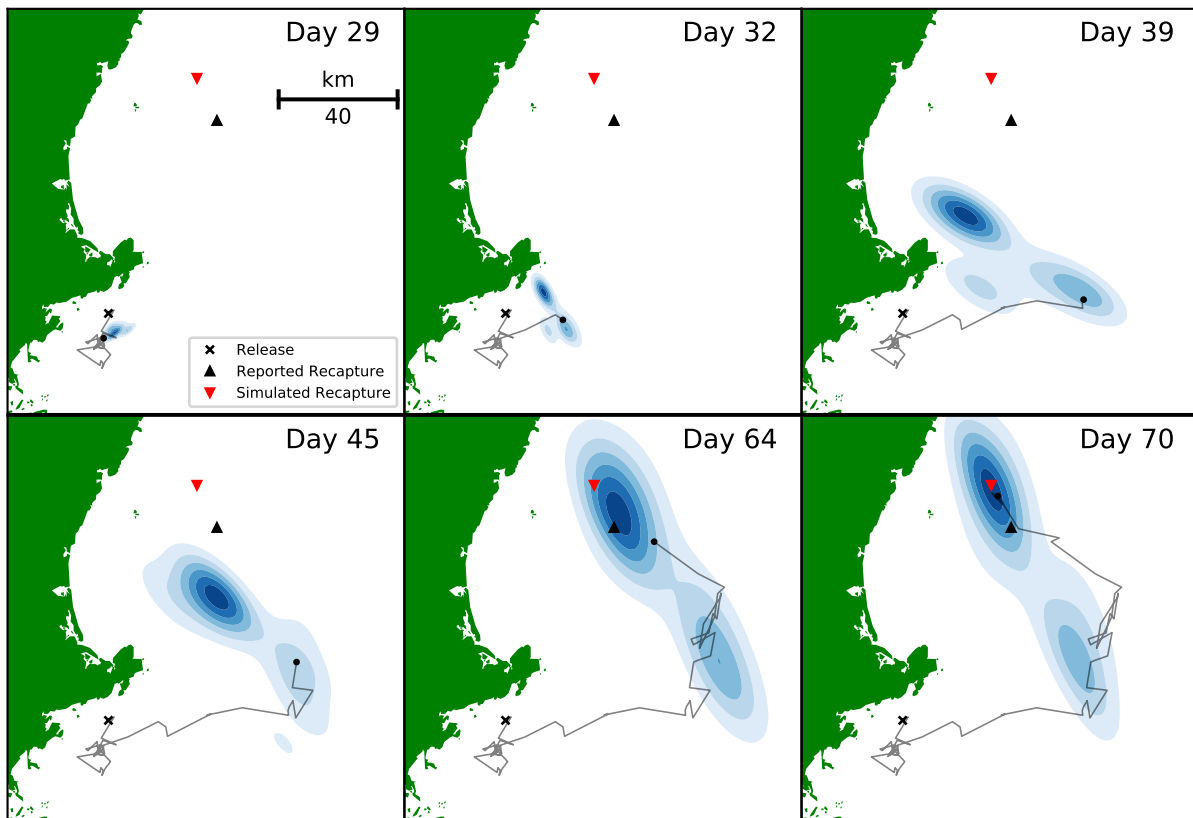


Figure 9: Progression of the daily posterior distribution (color rendering) and the most probable track (MPT, black line) for cod #17. Black cross: release location, black triangle: reported recapture location, red triangle: simulated recapture location.

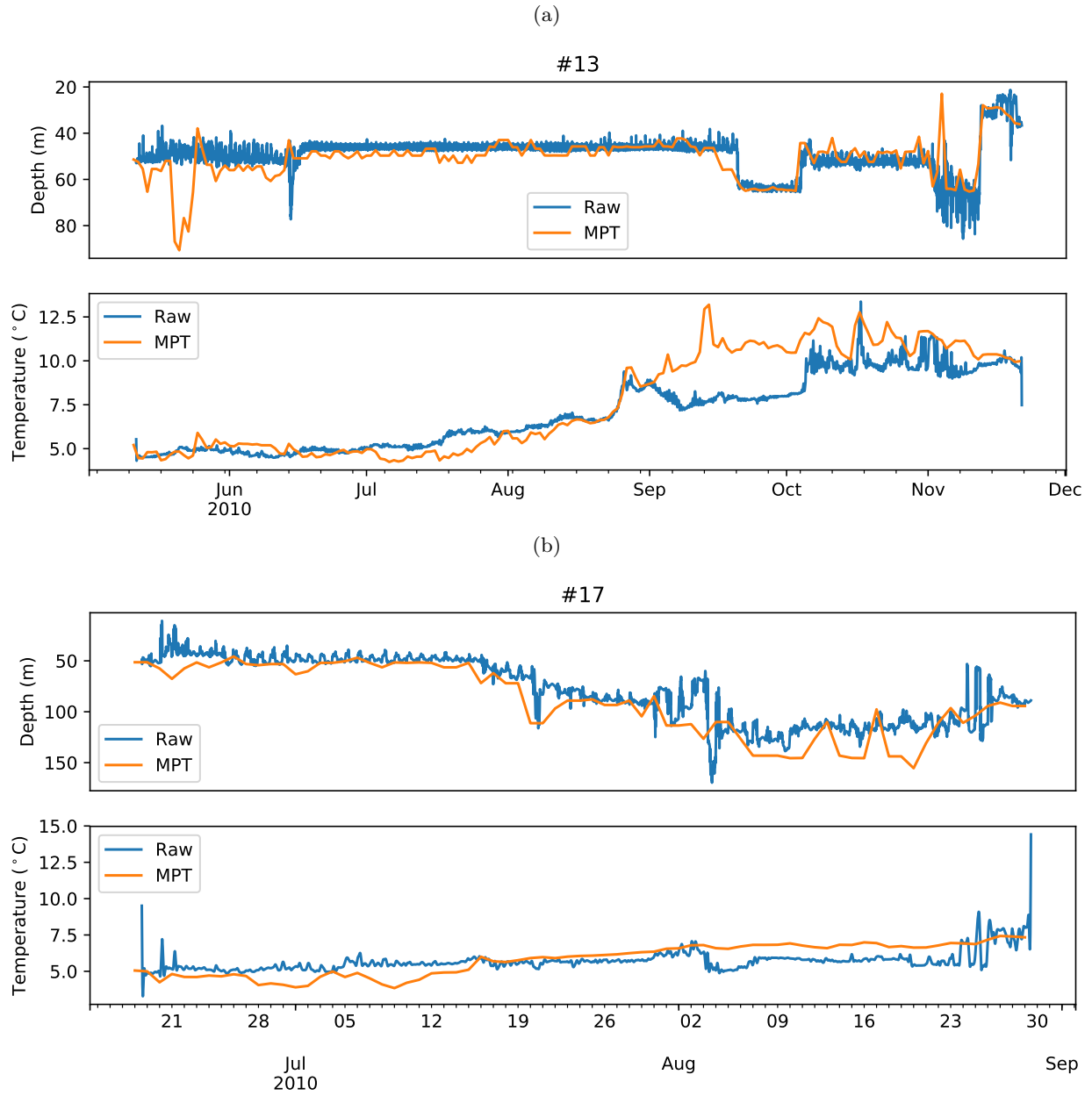


Figure 10: Comparison of the raw depth and temperature time series data recorded by the data storage tags (DSTs; blue line) and the daily depth and temperature data reconstructed from environmental database along the most probable track (MPT; orange line) for (a) cod #13 and (b) #17.



Table 1: Skills of the most probable track (MPT) of the PF geolocation method for mooring and double-tagging

| Data Source                             | Mooring          | Double-tagged fish |
|---|------------------|--------------------|
| # tag deployments                       | 14               | 10                 |
| # geolocation days with known locations | 762              | 222                |
| E2 Error range (km)                     | 0.01–27.53       | 0.29–46.77         |
| E2 RMS (km)                             | 14.95            | 18.19              |
| E2 Median (km)                          | 9.71             | 6.0                |
| E2 Mean $\pm$ S.D. (km)                 | 12.03 $\pm$ 8.87 | 12.47 $\pm$ 13.28  |
| E3 %days within 95% credible area       | 61.9             | 100                |

Table 2: Hardware specifications and PF-Throughput in geolocation-days per wall clock hour (d/h) on ten GPUs.

| NVIDIA GPU Model    | Architecture Generation | Compute Cores | Base Clock (MHz) | Memory Bandwidth (GB/s) | Single Precision GFLOPS | PF-Throughput (d/h) |
|---------------------|-------------------------|---------------|------------------|-------------------------|-------------------------|---------------------|
| Tesla V100          | Volta                   | 5120          | 1455             | 900.0                   | 14899.0                 | 1705                |
| Titan X             | Pascal                  | 3584          | 1417             | 480.0                   | 10157.0                 | 1090                |
| Tesla M60           | Maxwell                 | 4096          | 899              | 320.0                   | 7365.0                  | 877                 |
| Tesla K80           | Kepler                  | 4992          | 560              | 480.0                   | 5591.0                  | 657                 |
| GeForce GTX 1050 Ti | Pascal                  | 768           | 1290             | 112.1                   | 1981.4                  | 638                 |
| GeForce GTX 1050    | Pascal                  | 640           | 1354             | 112.0                   | 1733.1                  | 483                 |
| Tesla K40c          | Kepler                  | 2880          | 745              | 288.0                   | 4291.0                  | 413                 |
| GeForce GTX 750 Ti  | Maxwell                 | 640           | 1020             | 86.4                    | 1305.6                  | 391                 |
| GeForce GTX 560 Ti  | Fermi                   | 384           | 1645             | 128.0                   | 1263.4                  | 315                 |
| Tesla C2050         | Fermi                   | 448           | 1150             | 144.0                   | 1030.4                  | 228                 |